AGU PUBLICATIONS

JGR

Journal of Geophysical Research: Biogeosciences

RESEARCH ARTICLE
10.1002/2015JG002923

Key Points:
- Supratidal wetland functioned as CO_2 sink over 4 years in this study
- Episodic flooding suppressed daytime CO_2 uptake and nighttime CO_2 release
- Episodic flooding regulated light and temperature responses of NEE

Correspondence to:
G. Han and J. Yu,
gxhan@yic.ac.cn;
jbyu@yic.ac.cn

Citation:
Han, G., X. Chu, Q. Xing, D. Li, J. Yu, Y. Luo, G. Wang, P. Mao, and R. Rafique (2015), Effects of episodic flooding on the net ecosystem CO_2 exchange of a supratidal wetland in the Yellow River Delta, *J. Geophys. Res. Biogeosci.*, *120*, doi:10.1002/2015JG002923.

Received 17 JAN 2015
Accepted 13 JUL 2015
Accepted article online 16 JUL 2015

Effects of episodic flooding on the net ecosystem CO_2 exchange of a supratidal wetland in the Yellow River Delta

Guangxuan Han[1], Xiaojing Chu[1], Qinghui Xing[1], Dejun Li[2], Junbao Yu[1], Yiqi Luo[3], Guangmei Wang[1], Peili Mao[1], and Rashad Rafique[4]

[1]Key Laboratory of Coastal Environmental Processes and Ecological Remediation, Yantai Institute of Coastal Zone Research, Chinese Academy of Sciences, Yantai, China, [2]Institute of Subtropical Agriculture, Chinese Academy of Sciences, Changsha, China, [3]Department of Microbiology and Plant Biology, University of Oklahoma, Norman, Oklahoma, USA, [4]Joint Global Change Research Institute, Pacific Northwest National Laboratory, College Park, Maryland, USA

Abstract Episodic flooding due to intense rainfall events is characteristic in many wetlands, which may modify wetland-atmosphere exchange of CO_2. However, the degree to which episodic flooding affects net ecosystem CO_2 exchange (NEE) is poorly documented in supratidal wetlands of coastal zone, where rainfall-driven episodic flooding often occurs. To address this issue, the ecosystem CO_2 fluxes were continuously measured using the eddy covariance technique for 4 years (2010–2013) in a supratidal wetland in the Yellow River Delta. Our results showed that over the growing season, the daily average uptake in the supratidal wetland was −1.4, −1.3, −1.0, and −1.3 g C m^{-2} d^{-1} for 2010, 2011, 2012, and 2013, respectively. On the annual scale, the supratidal wetland functioned as a strong sink for atmospheric CO_2, with the annual NEE of −223, −164, and −247 g C m^{-2} yr^{-1} for 2011, 2012, and 2013, respectively. The mean diurnal pattern of NEE exhibited a smaller range of variation before episodic flooding than after it. Episodic flooding reduced the average daytime net CO_2 uptake and the maximum rates of photosynthesis. In addition, flooding clearly suppressed the nighttime CO_2 release from the wetland but increased its temperature sensitivity. Therefore, effects of episodic flooding on the direction and magnitude of NEE should be considered when predicting the ecosystem responses to future climate change in supratidal wetlands.

1. Introduction

Wetlands are widely recognized as one of the biggest unknowns regarding carbon dynamics and fluxes under climate change [*Paul et al.*, 2006; *Bonneville et al.*, 2008; *Erwin*, 2009]. Global climate change is predicted to increase the likelihood of potential changes in wetland ecosystem structure and function [*Millennium Ecosystem Assessment*, 2005], which in turn may change the carbon sink-source status of wetlands [*Aurela et al.*, 2004; *Syed et al.*, 2006]. As one of the most sensitive and vulnerable ecosystems to climate change [*Millennium Ecosystem Assessment*, 2005; *Bonneville et al.*, 2008; *Erwin*, 2009], wetlands also potentially pose a great feedback to future climate change because of their large soil carbon pools [*Mitsch and Gosselink*, 2007; *Mitsch et al.*, 2013]. Therefore, continuous, long-term field measurements of wetland-atmosphere carbon exchange are essential, as change in wetland hydrology or weather conditions will strongly affect carbon dynamics in these ecosystems under climate change [*Bonneville et al.*, 2008; *Jimenez et al.*, 2012].

The net ecosystem CO_2 exchange (NEE), the net result of the competing processes of gross primary production (GPP) and ecosystem respiration (R_{eco}), is a key measure used to examine the impact of meteorological variability on ecosystem carbon balance [*Teklemariam et al.*, 2010]. The micrometeorological eddy covariance (EC) technique has been widely used for quantifying NEE between the atmosphere and plant canopies in various wetland ecosystems, since it can provide continuous, long-term flux information integrated at the ecosystem scale [*Baldocchi*, 2003; *Urbanski et al.*, 2007]. At the end of the 1990s, some long-term CO_2 flux measurements using eddy covariance methods were started on wetlands [*Lafleur et al.*, 2003; *Aurela et al.*, 2004]. To date, eddy covariance measurements have been conducted to understand the carbon cycle in different wetland types, especially in peatlands, alpine wetlands, and tundra wetlands [e.g., *Yurova et al.*, 2007; *Sulman et al.*, 2010; *Hao et al.*, 2011; *Kang et al.*, 2014]. Depending on the wetland's chemical, biological, and physical characteristics, the NEE in the wetland varies substantially in space and

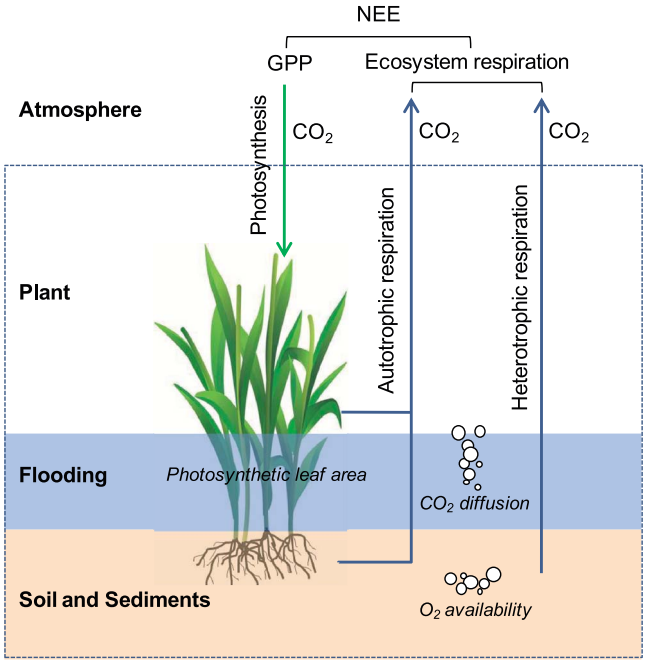

Figure 1. A schematic diagram illustrating the effect of flooding on the ecosystem CO_2 exchange in a wetland, including photosynthesis (gross primary production, GPP) and ecosystem respiration (i.e., the sum of autotrophic and heterotrophic respiration). NEE, net ecosystem CO_2 exchange, is the net result of the competing processes of GPP and ecosystem respiration. Flooding conditions may directly or indirectly affect the ecosystem CO_2 exchange by changing O_2 availability in soil, CO_2 diffusion in water column, and effective photosynthetic leaf area, which subsequently affect NEE in a wetland.

time [*Bonneville et al.*, 2008]. Thus, taking into account the diversity of wetland ecosystems, more studies should be conducted to include different wetland types in different climatic conditions [*Aurela et al.*, 2007]. However, there has been relatively few direct measurement of CO_2 exchange between coastal wetlands and the atmosphere at the ecosystem scale, regardless of their importance in balancing the global carbon budget [*Zhou et al.*, 2009; *Moffett et al.*, 2010; *Han et al.*, 2014b; *Xie et al.*, 2014].

The Yellow River Delta is one of the most active regions of land-ocean interaction among the large river deltas in the world. The interaction between fresh surface water, saline groundwater, and seawater in the Yellow River Delta has produced a variety of wetland types, plant communities, and ecological functions under different hydrological regimes [*Cui et al.*, 2009; *Fan et al.*, 2012]. The supratidal wetlands of the Yellow River Delta lie beyond the reach of the tides, and their hydrologic regimes are dominated by the interaction of precipitation, a shallow and saline water table, and marine sediments [*Yang et al.*, 2009; *Zhang et al.*, 2011]. During dry seasons, driven by strong evaporation, water-soluble salts from the groundwater are transported upward to the root zone and soil surface through capillary rise [*Yao and Yang*, 2010; *Zhang et al.*, 2011]. Consequently, most of the natural vegetation of the supratidal wetlands consists of salt tolerant herbs, grasses, and shrubs [*Han et al.*, 2014a]. However, during rainy season (from June to August), the episodic flooding is often observed, following heavy rainfall events [*Han et al.*, 2014a]. During the rainfall-driven episodic flooding, wetland water levels do not typically exceed 20 cm because much of the region is flat and there are many canals and ditches. Therefore, in supratidal zones of the Yellow River Delta, wetlands can become dry for long periods of time but can also experience short periods of rainfall-driven flooding lasting 1–2 months.

Episodic flooding conditions may directly or indirectly affect the uptake of CO_2 during photosynthesis (GPP) and the emissions of CO_2 via respiration as well as decomposition (R_{eco}) in several different aspects, which subsequently affect NEE in wetlands (Figure 1). On the one hand, when wetlands are inundated, the effective photosynthetic leaf area may be reduced as some plant leaves are submerged [*Schedlbauer et al.*, 2010; *Jimenez et al.*, 2012]. On the other hand, flooding causes displacement of gases when soil pores are filled with water, and soil hypoxia or anoxia can decrease overall plant metabolic activity and force stomatal closure and transpiration cessation, which affect plant photosynthesis and autotrophic respiration [*Banach et al.*, 2009; *Dušek et al.*, 2009; *Moffett et al.*, 2010; *Schedlbauer et al.*, 2010]. Furthermore, as soils become waterlogged, the saturation of surface soils limits the diffusion of oxygen into the wetlands, which limits microbial activity and decomposition rates of soil organic matter, leading to decrease in heterotrophic respiration [*Chivers et al.*, 2009; *Jimenez et al.*, 2012]. In addition, flooding conditions affect the sensitivity of CO_2 exchange to variation in light and temperature, which, in turn, influence the uptake of CO_2 in wetlands [*Polley et al.*, 2008; *Chivers et al.*, 2009]. The influence of flooding on CO_2 exchange is largely dependent on its characteristics (depth, frequency, duration, and starting date) in different wetland ecosystems [e.g., *Riutta et al.*, 2007; *Kathilankal et al.*, 2008; *Dušek et al.*, 2009; *Pelletier et al.*, 2011; *Jimenez et al.*, 2012; *Ballantyne et al.*, 2014]. It has been projected

that the frequency and intensity of heavy rainfall will increase under future climate change. As a result, precipitation-generated local flooding will increase in future [*Kundzewicz et al*., 2014]. Therefore, further information on the effects of rainfall-driven episodic floods on CO_2 exchange in wetlands becomes even more important in the context of global climate change [*Dušek et al*., 2009]. Such information is important not only for improving our knowledge on the mechanisms that control the CO_2 fluxes in wetlands but also for predicting possible impacts of climate change [*Aires et al*., 2008].

The rainfall-driven episodic inundation provided the opportunity to evaluate the response of net ecosystem CO_2 exchange to flooding stress. However, compared with the intertidal wetlands, the flooding in supratidal wetlands is not predictable. Transient floods in this area occur very quickly and with little warning due to intense rainfall events and shallow water tables, which increases the difficulty of collecting field data on wetland-atmosphere exchange during specific flood events [*Moffett et al*., 2010]. In order to evaluate the effect of rainfall-driven episodic flooding on the magnitude of NEE and its light and temperature response in the supratidal wetlands, we selected two adjacent periods, before and after flooding, each period including 10 days. We expected that episodic flooding affected NEE by altering GPP and ecosystem respiration. Based on a 4 year record (2010–2013) of CO_2 fluxes measured over a supratidal wetland in the Yellow River Delta, our objectives are (1) to characterize seasonal and interannual variations of NEE of the ecosystem and (2) to illustrate how the magnitude of NEE and its light and temperature response changed before and after episodic flooding over the 4 years.

2. Materials and Methods

2.1. Study Site

The Yellow River Delta, one of the largest deltas in China, is located in the southern bank of the Bohai Sea and the western Laizhou Bay. The evolution of the Yellow River Delta is influenced by the river discharge, suspended sediment load, changes of the river channel, and seawater intrusion [*Li et al*., 2009]. Due to the low elevation (generally below 10 m) and being near the sea, the hydrological characteristics in the Yellow River Delta are affected by the interactions between freshwater and seawater and between groundwater and surface water [*Cui et al*., 2009]. The groundwater table in this region is shallow with an average depth of 1.1 m [*Fan et al*., 2012], with a high level of groundwater mineralization averaging 30.1 g L^{-1} [*Yang et al*., 2009].

It has a warm-temperate and continental monsoon climate with distinctive seasons and distribution of rain and heat. The annual average temperature is 12.9°C, with minimum and maximum mean daily temperatures of −2.8°C in January and 26.7°C in July, respectively. The average annual precipitation is 560 mm, and about 74% is concentrated in the period of June to September. Annual average evaporation from water surface is 1962 mm, and the ratio of annual potential evaporation to precipitation is about 3.6:1. Large amounts of sand and sediment carried by the Yellow River have produced alternate depositional layers of sand and clay. The Yellow River Delta is covered mainly by extensive coverage of saline and wet soils.

The area of episodic waterlogged wetlands (i.e., heavily saline-alkalized wetlands) include *Phragmites australis* marshes, woodlands, shrub wetlands, and wet meadows [*Cui et al*., 2009]. The study was conducted in a supratidal wetland located on the Research Station of Coastal Wetland in the Yellow River Delta (37°45′50″N, 118°59′24″E), Chinese Academy of Sciences. The terrain of the station is quite flat with a sufficient fetch to meet the basic assumption for proper application of the EC technique. The vegetation is relatively homogeneous and strongly dominated by common reed (*Phragmites australis*), with other associated species including *Suaeda salsa*, *Tamarix chinensis*, *Imperata cylindrical*, and *Tripolium vulgare*. *Phragmites australis* usually bud around mid-April, head in mid-August, bloom around mid-September, and begin withering during early October. The maximum canopy height at the peak of the growing season (early July to mid-August) can reach up to 1.7 m, and the closure index was between 0.3 and 0.8. The growing season of the supratidal wetland ecosystem spans from May to October.

2.2. Eddy Covariance Measurements

Fluxes of CO_2 and water vapor (H_2O) between the supratidal wetland and the atmosphere were continuously measured using the EC methods [*Baldocchi*, 2003] from May 2010 to December 2013, including four growing seasons. The open-path EC system was mounted on the tower at a height of 2.8 m, and fetch length from all

directions was more than 300 m. More details about the measurement system are presented elsewhere [*Han et al*., 2014b]. The densities of CO_2 and H_2O were measured by an open-path infrared gas analyzer (IRGA, LI-7500, Li-COR Inc., USA), and the three wind components and the speed of sound were measured with a three-axis sonic anemometer (CSAT-3, Campbell Scientific Inc., USA). Raw data outputs from the IRGA and sonic anemometer were collected at 10 Hz and recorded by a data logger (CR1000, Campbell Scientific Inc., USA) at 30 min intervals. The IRGA was calibrated once or twice every year in the laboratory using pure nitrogen gas, CO_2 calibration gas, and a dew point generator (LI-610, Li-COR Inc., USA).

2.3. Meteorological Measurements

Continuous complementary measurements included standard meteorological and soil parameters around the flux tower. Net radiation was measured at a height of 3.0 m with a four-component net radiometer (CNR4, Kipp & Zonen USA Inc., Bohemia, NY, USA). Photosynthetically active radiation (PAR) was measured above the canopy at a height of 3.0 m using quantum sensors (LI-190SB, Li-COR Inc., USA). Air temperature and relative humidity were measured at the height of 2.5 m with a humidity and temperature probe (HMP45C, Vaisala, Helsinki, Finland). Wind speed and direction were measured at a height of 2.5 m with a propeller anemometer (034B, Campbell Scientific Inc., USA). Precipitation was measured with a tipping bucket rain gauge (TE525, Texas Electronics, Texas, USA). Soil volumetric water content was measured by time domain reflectometry probes (EnviroSMART SDI-12, Sentek Pty Ltd., USA) at seven depths (5 cm, 10 cm, 20 cm, 40 cm, 60 cm, 80 cm, and 100 cm). Soil temperature was measured at depths of 5, 10, 20, 30, and 50 cm using thermistors (109SS, Campbell Scientific Inc., USA). All meteorological data were monitored every 15 s and then averaged half hourly by a data logger (CR1000, Campbell Scientific Inc., USA).

2.4. Flux Data Processing and Quality Control

Raw data were processed using the postprocessing software EdiRe (University of Edinburg, Scotland) to determine net ecosystem CO_2 exchange with an averaged half hourly period. Corrections were made according to standard methods including despiking, coordinate rotation, time lag corrections, and air density corrections [*Webb et al*., 1980; *Kosugi et al*., 2008; *Schedlbauer et al*., 2010]. If the number of spikes or out-of-range data exceeded 1% of the total number of data points for each element, then the 30 min flux data samples were considered to be invalid [*Kosugi et al*., 2008]. A Webb-Pearman-Leuning correction for the effect of air density fluctuations [*Webb et al*., 1980] was applied. Furthermore, faked flux due to warming of IRGA at low temperature was also corrected for half-hour NEE data [*Yan et al*., 2010]. Subsequently, quality filtering was applied to eliminate half-hour flux data resulting from systematic errors according to the following rejection criteria: (1) incomplete half-hour measurements during system calibration or maintenance [*Jimenez et al*., 2012]; (2) excessive spikes in the sonic and IRGA data [*Schedlbauer et al*., 2010]; (3) precipitation, condensation, or bird fouling on the IRGA or sonic anemometer [*Lei and Yang*, 2010; *Schedlbauer et al*., 2010; *Jimenez et al*., 2012]; (4) biologically impossible values of NEE for the reed wetlands ($|NEE| > 60\ \mu mol\ CO_2\ m^{-2}\ s^{-1}$) [*Zhou et al*., 2009; *Han et al*., 2014b]; and (5) the flux data under nocturnal low atmospheric turbulence conditions were excluded based on friction velocity (u^*).

The eddy covariance technique has been recognized to underestimate the flux under low atmospheric turbulence conditions during the night [*Aires et al*., 2008; *Lei and Yang*, 2010; *Schedlbauer et al*., 2010]. We determined the u^* threshold using the method described by *Schedlbauer et al.* [2010]. The nighttime fluxes measured below u^* values of $0.15\ m\ s^{-1}$ were underestimated, so all half hourly NEE data with $u^* \leq 0.15\ m\ s^{-1}$ were rejected from the data sets. Negative nighttime CO_2 fluxes were also removed from the data sets. After this filtering process, the remaining data set performed the tests for stationarity and integral turbulent characteristics to detect unfavorable data [*Kaimal and Finnigan*, 1994; *Foken and Wichura*, 1996]. Following these screenings and tests, roughly 43% of the data obtained from the EC system was rejected during the whole study period. By convention, negative and positive NEE values represent sinks and sources of atmospheric CO_2, respectively.

2.5. Flux Gap Filling and Partitioning

In order to provide estimates for the balance of NEE, the data gaps were filled with the following procedure [*Lafleur et al*., 2003; *Sagerfors et al*., 2008; *Dušek et al*., 2009; *Hao et al*., 2011; *Han et al*., 2014b]. Small gaps (<2 h) were filled by linear interpolation using the neighboring measurements. For large gaps (≥2 h), the

missing NEE data were filled based on empirical models separately for daytime and nighttime data. Gap-filled half hourly fluxes were used to obtain an estimation of daily, monthly, and annual sums.

When PAR was $\geq$10 μmol m^{-2} s^{-1}, the missing daytime NEE data during the growing season were gap filled using the Michaelis-Menten model [*Falge et al.*, 2001], with an independent 10 day window:

$$\mathrm{NEE} = \frac{A_{\max}\alpha \mathrm{PAR}}{A_{\max} + \alpha \mathrm{PAR}} + R_{\mathrm{eco,\ day}} \quad (1)$$

where the coefficient α is the apparent quantum yield (μmol CO_2 μmol^{-1} photon), $A_{\max}$ is the light-saturated net CO_2 exchange (μmol CO_2 m^{-2} s^{-1}), $R_{\mathrm{eco,\ day}}$ is the daytime ecosystem respiration (μmol CO_2 m^{-2} s^{-1}), and PAR is the photosynthetically active radiation (μmol m^{-2} s^{-1}).

When PAR was $<$10 μmol m^{-2} s^{-1}, the missing nighttime NEE (i.e., nighttime ecosystem respiration, $R_{\mathrm{eco,\ night}}$) was filled using the van't Hoff empirical exponential function [*Lloyd and Taylor*, 1994]:

$$R_{\mathrm{eco,\ night}} = R_{10} Q_{10}^{(T-10)/10} \quad (2)$$

where R_{10} is the ecosystem respiration at a reference temperature of 10°C; T is the air or soil temperature (°C); and Q_{10}, the temperature sensitivity coefficient, is the rate of change in respiration for every 10°C. Correlation analysis revealed that ecosystem respiration was more significantly related to air temperature than soil temperature (data not shown). Thus, we only used the data of air temperature to investigate the influence of temperature on ecosystem respiration.

The CO_2 fluxes measured with the EC technique represent NEE, which is the result of gross primary production (GPP) and ecosystem respiration (R_{eco}). So the value of GPP can be calculated as the difference between R_{eco} and NEE [*Jacobs et al.*, 2007; *Schedlbauer et al.*, 2010]:

$$\mathrm{GPP} = R_{\mathrm{eco}} - \mathrm{NEE} \quad (3)$$

Daily R_{eco} is the sum of daytime ecosystem respiration ($R_{\mathrm{eco,\ day}}$) and the nighttime ecosystem respiration ($R_{\mathrm{eco,\ night}}$):

$$R_{\mathrm{eco}} = R_{\mathrm{eco,\ day}} + R_{\mathrm{eco,\ night}} \quad (4)$$

Based on the assumption that $R_{\mathrm{eco,\ day}}$ was of similar magnitude and responsiveness as $R_{\mathrm{eco,\ night}}$, $R_{\mathrm{eco,\ day}}$ was estimated by the extrapolation of the function relationship (equation (2)) developed for nighttime periods [*Lei and Yang*, 2010; *Schedlbauer et al.*, 2010].

2.6. Aboveground Biomass and Leaf Area Index

Aboveground biomass for the supratidal wetland was measured by harvesting the vegetation approximately every 2 weeks throughout the vegetative growth period (May–October) from 2011 to 2013. The sampling plot was 0.5 m × 0.5 m, and five replicates were taken on each measurement day. Live plants were clipped at 1 cm above the ground level. Plant aboveground biomass was oven dried for 48 h at 80°C before weighing. During the vegetative growth period from 2010 to 2013, the leaf area index (LAI) of the dominant species was also indirectly estimated at 2 week intervals in each plot using a portable meter (LI-2000, Li-COR, Inc., USA).

2.7. Statistical Analysis

Michaelis-Menten model was used to describe the relationships between daytime NEE and PAR, and exponential regression analysis was used to examine the relationships between nighttime NEE (R_{eco}) and air temperature. In order to analyze the effect of flooding on NEE, we selected four paired periods (before and after flooding, each period including 10 days). A two-tailed two-sample t test was used to test the significant differences in the magnitude of NEE, response of NEE to light (α, $A_{\max}$, and $R_{\mathrm{eco,\ day}}$), and response of R_{eco} to air temperature (R_{10} and Q_{10}) before and after episodic flooding over the 4 years. In all tests, a significance level of $P = 0.05$ was used.

3. Results

3.1. Meteorology, Aboveground Biomass, and LAI

Figure 2 shows the variation of the major meteorological conditions and plant parameters over the course of the study. Average daily R_n was 107.3, 115.0, and 113.1 W m^{-2} for 2011, 2012, and 2013, respectively. Average

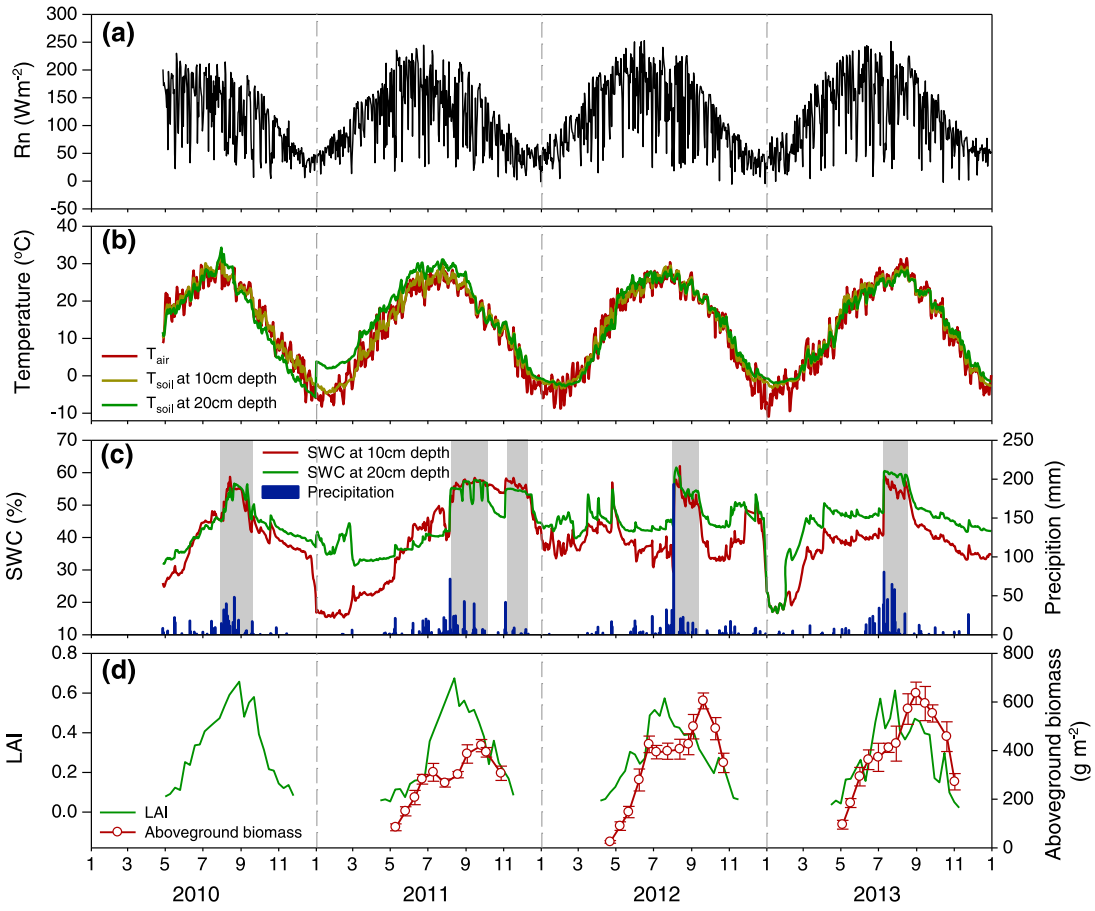

Figure 2. Seasonal and interannual variations of (a) daily net radiation (R_n), (b) air temperature (T_{air}) and soil temperature (T_{soil}) at 10 cm and 20 cm depths, (c) daily total precipitation and average volumetric soil water content (SWC) at 10 cm and 20 cm depths, and (d) leaf area index (LAI) and aboveground biomass for the period of 2010–2013 in a supratidal wetland. The gray shaded areas indicate the flooding periods.

daily R_n during the growth period (May to October) followed a similar trend with means 130.8, 136.6, 146.7, and 143.9 W m^{-2} in the years of 2010, 2011, 2012, and 2013, respectively. The air temperature in each year showed single-peak variation, and daily average air temperature ranged from −10.9°C in January 2013 to 31.6°C in July 2010 (Figure 2b). The air temperature during growing season followed a similar trend with means 21.4, 21.1, 21.8, and 21.9°C, for 2010, 2011, 2012, and 2013, respectively, which were near the 30 year (1978-2008) average (± standard deviation) (21.9 ± 1.6°C).

Precipitation was the environmental factor that differed markedly in study years due to both the amount and pattern of rain (Figure 2c). For example, precipitation in July of 2013 (384 mm) was 239% of the long-term average of 160 mm, but its precipitation in August (39 mm) was only about 30% of normal value of 134 mm. The total precipitation received during the growing season months in 2011 (496 mm) and 2012 (506 mm) were within one standard deviation of the 30 year average (± standard deviation) (486 ± 26 mm), whereas values in 2010 (433 mm) and 2013 (434 mm) were lower than the 30 year average precipitation. The variation in precipitation pattern resulted in seasonal and interannual variability in soil water content and episodic flooding (Figure 2c). Soil moisture (soil volumetric water content, SWC) presented a maximum in summer and a minimum in winter. With the onset of the rainy season at the end of June, soil moisture reached values constantly above 42%. Then a subsequent rain pulse that occurred in July and August led to episodic flooding in the wetland, and the flooding duration lasted varied 1–2 months in each study year (Figure 2c).

Aboveground biomass and LAI are primarily dependent on seasonal fluctuations in temperature and precipitation time and quantity (Figure 2d). The value of aboveground biomass increased rapidly in May and

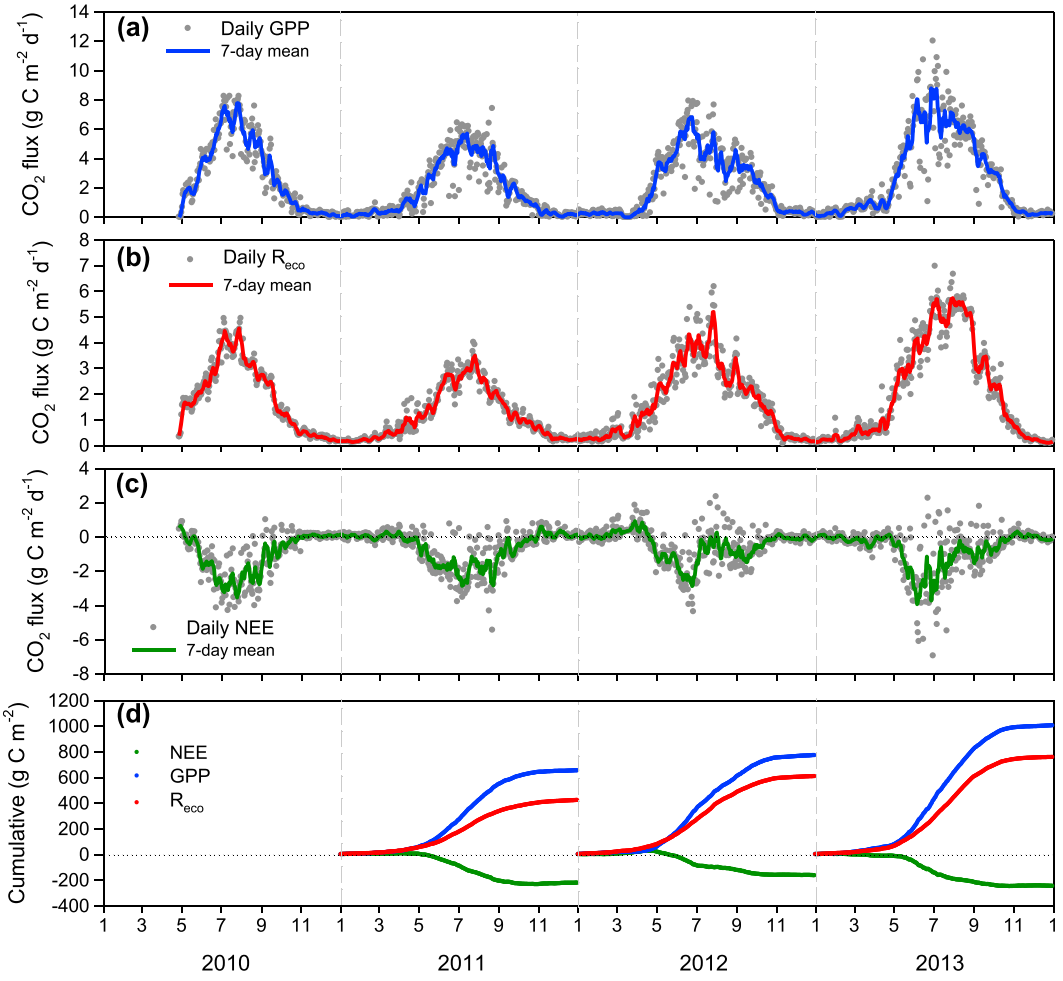

Figure 3. Seasonal variation in daily average (a) gross primary production (GPP); (b) ecosystem respiration (R_{eco}); (c) net ecosystem CO_2 exchange (NEE); and (d) the cumulative GPP, R_{eco}, and NEE over the period of 2010–2013 in a supratidal wetland. Each dot represents 1 day. The lines represent the running mean.

reached a maximum between August and September, followed by a gradual decline as the wetland senesced during October and November (Figure 2d). The seasonal peak value of aboveground biomass was 425 $\pm$ 25 g m^{-2} in late September of 2011, 604 $\pm$ 33 g m^{-2} in mid-September of 2012, while in 2013 the peak was 636 $\pm$ 46 g m^{-2} in early August. Values of LAI across years showed a very similar seasonal response. The LAI was low in winter and spring, then increased during plant green-up in May to a peak in July or August, and then decreased as plants senesced in autumn. In addition, periods of peak LAI differed slightly among years but generally occurred during the mid-July to late-August period. Maximum values of LAI were 0.66, 0.67, 0.57, and 0.61 in 2010, 2011, 2012, and 2013, respectively. In the study years, the peak of LAI was about a month earlier than the peak of aboveground biomass.

3.2. Seasonal and Interannual Variations of Ecosystem CO_2 Exchange

The courses of ecosystem CO_2 fluxes (Figures 3a–3c) showed significant seasonal variations, with a net sink of CO_2 during the growing season (May–October) and a net source of CO_2 for the remainder of the year (November–April), which were closely related to meteorological conditions and vegetation phenology. In each year, both GPP and R_{eco} showed an asymmetric bell shape.

Daily values for NEE over the course of the study ranged from an uptake of -7.0 g C m^{-2} d^{-1} in late June of 2013 to a loss of 2.4 g C m^{-2} d^{-1} in late July of 2012. During the early growing season (from late April to early May), with the seed germination and increasing leaf area deployment (Figure 2d), GPP and R_{eco} increased

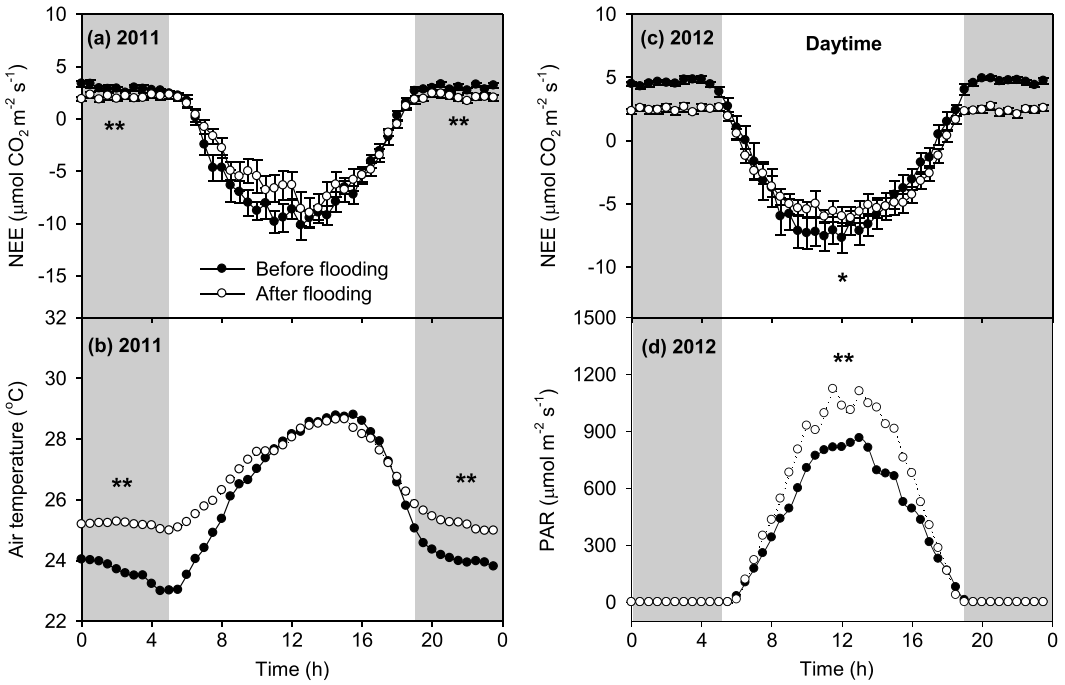

Figure 4. The effects of episodic flooding on the diurnal pattern of 10 day average net ecosystem CO_2 exchange (NEE) and environmental factors in (a and b) 2011 and (c and d) 2012, respectively. Significant difference in (Figure 4a) nighttime NEE and (Figure 4b) air temperature during the after-flooding period (open circles) compared to the before-flooding (closed circles) period in 2011. Significant difference in (Figure 4c) daytime NEE and (Figure 4d) PAR during the before-flooding (closed circles) period compared to the after-flooding period (open circles) in 2012. The gray shaded areas indicate nighttime. Values of NEE represent the mean ±SE. *: $P < 0.05$; **: $P < 0.01$.

gradually, the wetland ecosystem became a daily carbon sink (negative NEE) as rates of photosynthesis become greater than respiration rates. During the main growing season (from mid-May to early Ocotober), GPP and R_{eco} increased steadily, with an increasing dominance of GPP over R_{eco} (Figures 3a and 3b). As a consequence, daily NEE was high negative value (a net carbon sink) and remained negative until November (Figure 3c). In that period, the values of NEE reached their maximum of $-4.3\,g\,C\,m^{-2}\,d^{-1}$ in mid-July of 2010, $-5.4\,g\,C\,m^{-2}\,d^{-1}$ in late August of 2011, $-4.4\,g\,C\,m^{-2}\,d^{-1}$ in late June of 2012, and $-7.0\,g\,C\,m^{-2}\,d^{-1}$ in late June of 2013, respectively. The maximum daily values of R_{eco} did not correspond to the days with the peak GPP but lagged several days instead, occurring later after the highest GPP values with the evolution of temperature. In addition, very small values of NEE appeared occasionally from July to September, which always occurred during rainy or cloudy days with low PAR. At the end of the senescence of vegetation, GPP and R_{eco} gradually decreased, following the reductions in R_n and T_{air} (Figures 2a and 2b) and the decrease of LAI of the vegetation (Figure 2d).

Overall, the daily average uptake over the growing season in the supratidal wetland was 1.4, 1.3, 1.0, and $1.3\,g\,C\,m^{-2}\,d^{-1}$ for 2010, 2011, 2012, and 2013, respectively. On the annual scale, the cumulative GPP, R_{eco}, and NEE in all 3 years (2011−2013) showed a high variation (Figure 3d). The annual cumulative NEE were −223, −164, and $-247\,g\,C\,m^{-2}$ for 2011, 2012, and 2013, respectively. Those for annual GPP were 653, 772, and $1004\,g\,C\,m^{-2}$ for 2011, 2012, and 2013, respectively; for annual R_{eco}, they were 430, 608, and $757\,g\,C\,m^{-2}$ for 2011, 2012, and 2013, respectively.

3.3. Effect of Episodic Flooding on the Magnitude of NEE

Figure 4 shows the impact of episodic flooding on the diurnal pattern of NEE averaged over 10 day periods before and after flooding in 2011 and 2012, respectively. For both years, the mean diurnal patterns of measured NEE before and after flooding were very similar in shape but varied substantially in amplitude (Figures 4a and 4c). Average NEE after flooding exhibited a smaller range of variation than that before flooding, with net carbon loss during the nighttime and net carbon uptake during the daytime. In 2011, nighttime NEE

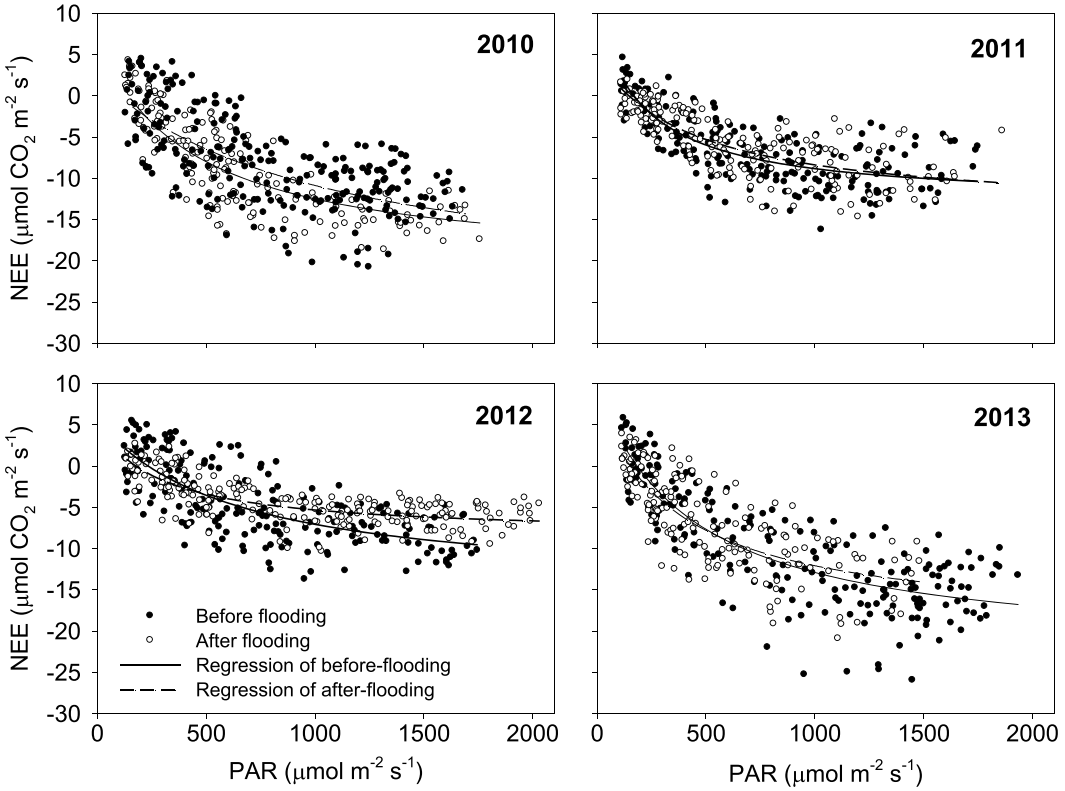

Figure 5. Comparison of the light-response curves for net ecosystem CO_2 exchange (NEE) during the before-flooding (closed circles) and after-flooding (open circles) periods in 2010, 2011, 2012, and 2013. Each before-flooding and after-flooding periods include 10 days. The curves were fitted using a rectangular hyperbola equation (equation (1)), and regression coefficients are presented in Table 1.

(shaded area in Figure 4a) after flooding (2.0 ± 0.1 μmol CO_2 m^{-2} s^{-1}) was significantly reduced by 29% compared to that before flooding (2.8 ± 0.1 μmol CO_2 m^{-2} s^{-1}), although its air temperature was significantly higher than that before flooding ($P < 0.01$; Figure 4b). Therefore, it seems likely that the episodic flooding suppressed the nighttime CO_2 release from the supratidal wetland. Meanwhile, in 2012 the average daytime CO_2 uptake after flooding (-5.6 ± 0.4 μmol CO_2 m^{-2} s^{-1}) was also significantly reduced by 13% (Figure 4c) compared to that before flooding (-4.9 ± 0.2 μmol CO_2 m^{-2} s^{-1}). However, PAR after flooding was on average 682.1 $\pm$ 69.2 μmol m^{-2} s^{-1}, significantly higher ($P < 0.01$) than that before flooding (524.6 ± 51.4 μmol m^{-2} s^{-1}; Figure 4d), indicating that the episodic flooding reduced daytime CO_2 uptake in supratidal wetlands.

3.4. Effect of Episodic Flooding on Response of NEE to Light

The impact of the episodic flooding on the response curves of NEE to PAR from 2010 to 2014 is shown in Figure 5. The relationship between NEE and PAR was well described by a rectangular hyperbolic function (equation (1)) for both before- and after-flooding periods in all study years ($P < 0.01$; Figure 5 and Table 1). There was a significant difference between two conditions in the parameter A_{max} of the model between NEE and PAR ($P < 0.01$; Table 1). On average A_{max} after flooding was lower than during before flooding (21.3 and 27.4 μmol CO_2 m^{-2} s^{-1}, respectively). The A_{max} was substantially reduced after the episodic flooding, which is consistent with the decrease in daytime CO_2 uptake that followed the episodic flooding (Figure 4). In addition, on average the parameter $R_{eco,day}$ after flooding (6.4 ± 1.5 μmol CO_2 m^{-2} s^{-1}) was lower than the value before flooding (9.3 ± 2.7 μmol CO_2 m^{-2} s^{-1}), although the difference was not significant ($P = 0.09$; Table 1). In general, the parameter α showed little difference between the before- and afer-flooding periods ($P > 0.05$).

3.5. Effect of Episodic Flooding on Response of R_{eco} to Air Temperature

We also compared the effect of the episodic flooding on the response of ecosystem respiration (R_{eco}) to air temperature in the supratidal wetland from 2010 to 2013 (Figure 6 and Table 2). R_{eco} was positively related to

Table 1. Comparison of Coefficients α, A_{max}, and $R_{eco,\ day}$ Estimated Using Equation (1) and Their Paired Sample *t* Test Before and After Flooding in a Supratidal Wetland Over the Period of 2010–2013 in a Supratidal Wetland[a]

	α (μmol μmol^{-1})		A_{max} (μmol CO_2 m^{-2} s^{-1})		$R_{eco,\ day}$ (μmol CO_2 m^{-2} s^{-1})		R^2	
Year	Before Flooding	After Flooding	Before Flooding	After Flooding	Before Flooding	After Flooding	Before Flooding	After Flooding
2010	0.099 ± 0.030	0.061 ± 0.032	33.8 ± 2.1	25.3 ± 2.1	12.0 ± 3.2	7.3 ± 3.5	0.74	0.49
2011	0.107 ± 0.052	0.048 ± 0.021	23.1 ± 2.8	18.6 ± 1.3	10.2 ± 3.5	5.2 ± 2.1	0.62	0.6
2012	0.033 ± 0.013	0.047 ± 0.024	20.6 ± 1.4	13.5 ± 1.7	5.6 ± 1.8	5.2 ± 2.2	0.54	0.57
2013	0.073 ± 0.024	0.075 ± 0.035	32.3 ± 1.6	27.7 ± 1.9	9.5 ± 2.6	8.1 ± 3.3	0.72	0.61
Mean	0.078 ± 0.033	0.058 ± 0.013	27.4 ± 6.6	21.3 ± 6.4	9.3 ± 2.7	6.4 ± 1.5		
t test	1.188		6.3[b]		2.5			

[a]Parameter α is the ecosystem apparent quantum yield, A_{max} is the ecosystem light-saturated net CO_2 exchange, $R_{eco,\ day}$ is the ecosystem respiration in the daytime estimated from the NEE-PAR response curve, *n* is the number of observations, and R^2 is the coefficient of determination. Values of coefficients represent the mean ±SE.

[b]$P < 0.05$, *t* test; $P < 0.01$, *t* test.

air temperature and could be expressed by the exponential function for both before- and after-flooding periods in all study years ($P < 0.01$). The temperature sensitivity coefficient R_{10} before flooding (2.2) was significantly greater ($P < 0.01$) than that after flooding (0.7), indicating the episodic flooding decreasing the basal respiration of a supratidal wetland. However, the temperature sensitivity coefficient Q_{10} before flooding (1.5) was significantly lower ($P < 0.01$) than that after flooding (2.6). Comparison of Q_{10} under two conditions suggests that the episodic flooding increased Q_{10} of ecosystem respiration in a supratidal wetland. Thus, the ecosystem respiration after flooding was more sensitive to the change of air temperature than that before flooding.

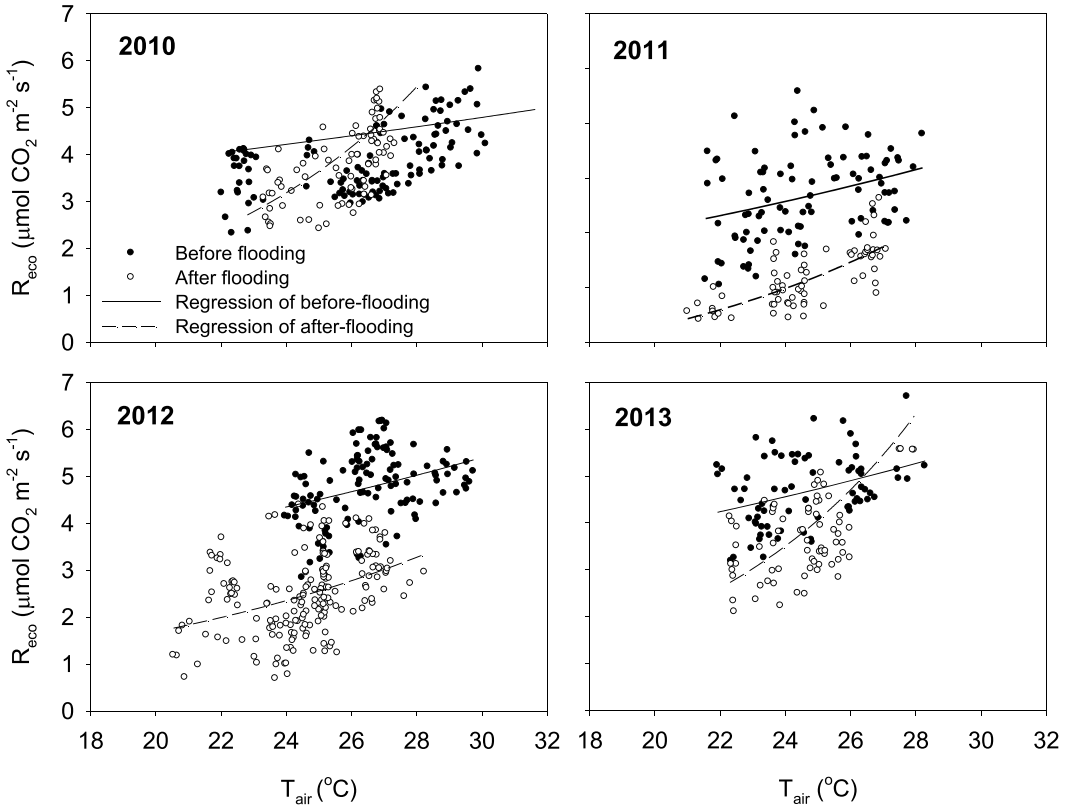

Figure 6. Comparison of the temperature-response curves for nighttime NEE (ecosystem respiration, R_{eco}) during the before-flooding (closed circles) and after-flooding (open circles) periods in 2010, 2011, 2012, and 2013. Each before-flooding and after-flooding periods include 10 days. The curves were fitted using equation (2), and the regression coefficients are presented in Table 2.

Table 2. Values of Coefficients R_{10} and Q_{10} of the Equation ($R_{eco,\ night} = R_{10}Q_{10}^{(T\text{-}10)/10}$) and Their Paired Sample *t* Test Before and After Flooding Over the Period of 2010–2013 in a Supratidal Wetland of the Yellow River Delta, China

	R_{10}		Q_{10}		R^2		P	
Year	Before Flooding	After Flooding	Before Flooding	After Flooding	Before Flooding	After Flooding	Before Flooding	After Flooding
2010	2.05	0.71	1.46	2.86	0.25	0.39	<0.001	<0.001
2011	1.86	0.48	1.56	2.80	0.14	0.53	<0.001	<0.001
2012	2.39	0.64	1.51	2.46	0.14	0.15	<0.001	<0.001
2013	2.65	0.97	1.46	2.44	0.14	0.28	0.001	<0.001
Mean	2.22	0.71	1.50	2.64				
t test	14.81[a]		−10.61[b]					

[a] $P < 0.05$, *t* test.
[b] $P < 0.01$, *t* test.

4. Discussion

4.1. Annual Ecosystem CO_2 Budget

In the supratidal wetland, the annual NEE budgets between −164 and −247 g C m^{-2} yr^{-1} are in accordance with the results of earlier studies, showing most wetland ecosystems acting as a net uptake of CO_2 (Table 3). The annual net uptake of CO_2 of the supratidal wetland is comparable to values reported for temperate cattail marsh [*Bonneville et al*., 2008] and temperate sedge-grass marsh [*Dušek et al*., 2009]. In addition, the carbon budgets determined in this study is higher than the average net annual uptake of a tidal wetland (65 g C m^{-2} yr^{-1}) in northeast China [*Zhou et al*., 2009] and lower than that of an estuary wetland (639 g C m^{-2} yr^{-1}) in the Yangtze River estuary of China [*Yan et al*., 2010]. The differences in annual NEE between locations might be attributable to climatic conditions, hydrologic regime (e.g., flood magnitude, duration, frequency, and timing), nutrient availability, and vegetation [*Law et al*., 2001; *Kathilankal et al*., 2008; *Dušek et al*., 2009; *Zhou et al*., 2009]. Based on recent literature on carbon storage and fluxes within freshwater wetlands, *Kayranli et al.* [2010] indicate that wetlands can be both sources and sinks of carbon, depending on their age, operation, and the environmental boundary conditions such as location and climate. Across 11 different ecosystems types in sub-Saharan Africa, the maximum carbon assimilation rates were highly correlated with mean annual rainfall [*Merbold et al*., 2009]. Across 12 northern peatland and tundra sites in northern Europe and North America, annual GPP and NEE correlated significantly with LAI and pH [*Lund et al*., 2010]. However, by examining midsummer CO_2 fluxes measured above 7 northern peatlands, *Humphreys et al.* [2006] found that NEE was similar among most of the sites despite large differences in water table depth, water chemistry, and plant communities.

In addition, there was large interannual fluctuation in NEE in the supratidal wetland (Figure 3). Some studies have shown significant interannual variability in net CO_2 exchange in different wetland types. For example, in a freshwater marsh, the NEE over 5 years (1999–2003) demonstrated large interannual variability, ranged from −251 g C m^{-2} yr^{-1} in 2000 to 515 g C m^{-2} yr^{-1} in 2001 [*Rocha and Goulden*, 2008]. Interannual variations of the CO_2 balance in wetlands are likely related to the direct effects of climate variability [*Aurela et al*., 2004], plant phenology [*Lafleur et al*., 2003], water table position [*Yurova et al*., 2007; *Ballantyne et al*., 2014], and shifts in wetland production efficiency [*Rocha and Goulden*, 2008]. For example, in a subarctic fen the snowmelt timing is the most important single determinant of the annual carbon balance [*Aurela et al*., 2004]. A pronounced reduction in salt marsh-atmosphere CO_2 exchange during tidal flood events was in proportion to flood duration [*Moffett et al*., 2010]. However, in a freshwater marsh, interannual variation in carbon exchange resulted from shifts in the marsh's production efficiency (net CO_2 exchange per LAI) that were not caused by changes in wetland hydrology or weather conditions [*Rocha and Goulden*, 2008]. Therefore, more long-term data sets are required to better determine the annual cycle and interannual variability in NEE and identify its controlling factors.

4.2. Episodic Flooding Controls on Ecosystem CO_2 Exchange

Our results show that episodic flooding conditions reduced daytime uptake rate of CO_2 (Figure 4c) and the maximum rates of photosynthesis (Table 1), maybe owing to reduced rates of photosynthetic carbon fixation. The same results have been found in a short-hydroperiod marsh [*Schedlbauer et al*., 2010], a temperate sedge-grass marsh [*Dušek et al*., 2009], and a freshwater marsh [*Jimenez et al*., 2012]. During flooding events, the

Table 3. Comparison of Ecosystem CO_2 Exchange Among Different Wetland Ecosystems Across the Globe[a]

Wetland Types	Location	Latitude	Longitude	Period of Observation	Annual Air Temperature (°C)	Annual Precipitation (mm)	NEE	GPP	R_{eco}	Reference
Temperate sedge-grass marsh	South Bohemia, Czech Republic	49°01′N	14°46′E	2006	7.9	713	−199	-	-	*Dušek et al.* [2009]
				2007	9.1	586	−220	-	-	
Temperate cattail marsh	Ontario, Canada	45°24′N	75°30′W	2005–2006	7.6	896	−264	831	567	*Bonneville et al.* [2008]
Freshwater tidal wetland	The Liaohe Delta, China	41°08′N	121°54′E	2005	8.3	631	−65	1257	1192	*Zhou et al.* [2009]
Flooded restored wetland (Old)	The Sacramento-San	38°06′N	121°39′W	2012–2013	15.6	278	−397	1506	1108	*Knox et al.* [2015]
Flooded restored wetland (Young)	Joaquin Delta, USA	38°03′N	121°45′W	2012–2013	15	390	−368	2106	1834	
Freshwater marsh	Southern California, USA	33°39′N	117°51′W	1999–2003	16.6	266	−251~515	1090~1639	1313~1632	*Rocha and Goulden* [2008]
Freshwater marsh	Everglades, USA	25°26′N	80°35′W	2008	23.7	1206	−78.8	468	389	*Jimenez et al.* [2012]
				2009		1284	−11	456	445	
		25°33′N	80°47′W	2009	24.6	1090	−80	361	442	
Tropical peat swamp forest	Central Kalimantan, Indonesia	21°21′S	114°12′E	2002	26.7	1852	602	3246	3848	*Hirano et al.* [2007]
				2003	26.4	2292	382	3461	3844	
				2004	25.9	2560	313	3594	3907	
Supratidal wetland	The Yellow River Delta, China	37°46′N	118°59′E	2011	12	600	−223	653	430	This study
				2012	12	615	−164	772	608	
				2013	12.1	634	−247	1004	757	

[a]NEE, GPP, and R_{eco} in g C m^{-2} yr^{-1}. NEP used where NEE unavailable.

effective photosynthetic leaf area may be reduced as the shoots and leaves are partially or completely submerged [*Schedlbauer et al.*, 2010; *Jimenez et al.*, 2012]. Meanwhile, diffusion of gases in water is approximately 10^4-fold slower than in air [*Vogel*, 1994]; therefore, slow entry of CO_2 into leaves typically limits photosynthesis [*Colmer et al.*, 2011]. In addition to severe CO_2 limitation, the photosynthesis of inundated leaves can also be limited by light, in particular when the flooding water is turbid [*Colmer et al.*, 2011; *Hidding et al.*, 2014]. Moreover, the low diffusion rate of oxygen in water results in limitation of oxygen availability for plant roots. As a consequence, hypoxia or anoxia conditions lead to a switch of aerobic metabolism of plants into less efficient anaerobic fermentation [*Bailey-Serres and Voesenek*, 2008], which can have a negative impact on plant photosynthesis and growth [*Sairam et al.*, 2008]. Thus, when the leaves of *Phragmites australis* are submerged, underwater net photosynthesis is greatly reduced following flooding [*Colmer et al.*, 2011]. However, inflow of freshwater after heavy rains tends to dilute the salinity in the supratidal wetland, which may promote the growth of the dominant halophytic species and consequently increase CO_2 uptake. For example, the flooding in an Alaskan rich fen increased ecosystem carbon storage due largely to increased early season gross primary production and higher light-saturated photosynthesis [*Chivers et al.*, 2009].

Our results also show that flooding clearly suppressed the nighttime CO_2 release (ecosystem respiration) from the supratidal wetland but increased its temperature sensitivity Q_{10} (Figure 4a and Table 2). Similarly, Everglades mangrove forests exhibited lower respiration rates during inundation [*Barr et al.*, 2010]. Also, compared to the control plot in an Alaskan rich fen, the flooded treatment had lower maximum respiration rates but a higher Q_{10} of ecosystem respiration [*Chivers et al.*, 2009]. Flooding can occur with various combinations of chemical and physical properties (O_2, temperature, pH, and light) in the soil and water [*Colmer et al.*, 2011]. There are several potential mechanisms that could have contributed to the suppression of ecosystem respiration following flooding.

On the one hand, when soil is inundated, the saturation of surface soils limits the diffusion of oxygen into the wetlands. Thus, lower O_2 availability and inhibition of aerobic respiration lead to lower CO_2 emissions [*Jimenez et al*., 2012; *McNicol and Silver*, 2014]. On the other hand, due to slow diffusion rate of CO_2 in water, the diffusive boundary layer resistance can limit rates of CO_2 emission through the surface water [*Vogel*, 1994]. Therefore, wetland inundation generally is expected to decrease CO_2 emissions to the atmosphere. However, previous studies also found that flooding had no marked effect on ecosystem respiration in some wetland ecosystems [*Dušek et al*., 2009; *Tong et al*., 2014] depending on site and vegetation characteristics [*Chivers et al*., 2009].

Episodic floods due to intense rainfall events are characteristic of many wetlands [*Moffett et al*., 2010]. Changes in rainfall frequency and intensity will significantly change periods of inundation, which may strongly affect carbon dynamics in these wetland ecosystems [*Jimenez et al*., 2012]. Variation in water level, flooding frequency, and duration can have multidimensional and synergistic effects on CO_2 exchange in wetlands, leading to a shift of carbon sink source [*Riutta et al*., 2007; *Moffett et al*., 2010; *Jimenez et al*., 2012; *Ballantyne et al*., 2014; *Xie et al*., 2014]. Furthermore, wetland microforms and vegetation composition also affect the response of CO_2 fluxes to flooding [*Schedlbauer et al*., 2010; *Pelletier et al*., 2011]. Therefore, it is necessary to carry out further measurements to assess the long-term effect of flooding on the wetland ecosystem CO_2 exchanges in this region.

5. Conclusions

This study demonstrated that episodic flooding reduced the average daytime net CO_2 uptake and the maximum rates of photosynthesis. In addition, flooding clearly suppressed the nighttime CO_2 release but increased its temperature sensitivity. These results emphasize that episodic flooding will modify the magnitude of NEE and its response to light and temperature in supratidal wetlands. However, in our study the effect of flooding on NEE was only observed during the four paired periods before and after flooding (each period including 10 days) and did not hold the entire flooding periods over 4 years. Additionally, surface water depth was not measured during the flooding periods. These limited data will increase the uncertainty about the effect of episodic flooding on NEE in the supratidal wetland. Moreover, flooding exerts disproportionate influence on export of dissolved and particulate organic carbon and especially CH_4 emission. Hence, further research and more continuous data sets of carbon exchange, wetland hydrology, and other environmental factors are needed to understand how carbon exchange respond to flooding and to assess the direction and magnitude of future carbon changes in supratidal wetlands.

Acknowledgments

This research was funded by the National Natural Science Foundation of China (41301083 and 41301052) and the National Science and Technology Support Program of China (2011BAC02B01). We wish to thank Liqiong Yang, Huabing Li, Yuhong Liu, Baohua Xie, and Bo Guan for their helpful work during this study. We also thank two anonymous reviewers for their expert advice and fruitful comments that significantly improved the paper. The data used in this study can be accessed by contacting the corresponding author.

References

Aires, L. M. I., C. A. Pio, and J. S. Pereira (2008), Carbon dioxide exchange above a Mediterranean C3/C4 grassland during two climatologically contrasting years, *Global Change Biol.*, *14*, 539–555.

Aurela, M., T. Laurila, and J. P. Tuovinen (2004), The timing of snow melt controls the annual CO_2 balance in a subarctic fen, *Geophys. Res. Lett.*, *31*, L16119, doi:10.1029/2004GL020315.

Aurela, M., T. Riutta, T. Laurila, J. P. Tuovinen, T. Vesala, E. S. Tuittila, J. Rinne, S. Haapanala, and J. Laine (2007), CO_2 exchange of a sedge fen in southern Finland—The impact of a drought period, *Tellus, Ser. B*, *59*, 826–837.

Bailey-Serres, J., and L. A. C. J. Voesenek (2008), Flooding stress: Acclimations and genetic diversity, *Annu. Rev. Plant Biol.*, *59*, 313–339.

Baldocchi, D. D. (2003), Assessing the eddy covariance technique for evaluating carbon dioxide exchange rates of ecosystems: Past, present and future, *Global Change Biol.*, *9*, 479–492.

Ballantyne, D. M., J. A. Hribljan, T. G. Pypker, and R. A. Chimner (2014), Long-term water table manipulations alter peatland gaseous carbon fluxes in Northern Michigan, *Wetlands Ecol. Manage.*, *22*, 35–47.

Banach, K., A. M. Banach, L. P. M. Lamers, H. de Kroon, R. P. Bennicelli, A. J. M. Smits, and E. J. W. Visser (2009), Differences in flooding tolerance between species from two wetland habitats with contrasting hydrology: Implications for vegetation development in future floodwater retention areas, *Ann. Bot.*, *103*, 341–351.

Barr, J. G., V. Engel, J. D. Fuentes, J. C. Zieman, T. L. O'Halloran, T. J. Smith, and G. H. Anderson (2010), Controls on mangrove forest-atmosphere carbon dioxide exchanges in western Everglades National Park, *J. Geophys. Res.*, *115*, G02020, doi:10.1029/2009JG001186.

Bonneville, M. C., I. B. Strachan, E. Humphreys, and N. T. Roulet (2008), Net ecosystem CO_2 exchange in a temperate cattail marsh in relation to biophysical properties, *Agric. For. Meteorol.*, *148*, 69–81.

Chivers, M. R., M. R. Turetsky, J. M. Waddington, J. W. Harden, and A. D. McGuire (2009), Effects of experimental water table and temperature manipulations on ecosystem CO_2 fluxes in an Alaskan rich fen, *Ecosystems*, *12*, 1329–1342.

Colmer, T. D., A. Winkel, and O. Pedersen (2011), A perspective on underwater photosynthesis in submerged terrestrial wetland plants, *AoB Plants*, *2011*, plr030.

Cui, B., Q. Yang, Z. Yang, and K. Zhang (2009), Evaluating the ecological performance of wetland restoration in the Yellow River Delta, China, *Ecol. Eng.*, *35*, 1090–1103.

Dušek, J., H. Čížková, R. Czerný, K. Taufarová, M. Šmídová, and D. Janouš (2009), Influence of summer flood on the net ecosystem exchange of CO_2 in a temperate sedge-grass marsh, *Agric. For. Meteorol.*, *149*, 1524–1530.

Erwin, K. L. (2009), Wetlands and global climate change: The role of wetland restoration in a changing world, *Wetlands Ecol. Manage.*, *17*, 71–84.

Falge, E., et al. (2001), Gap filling strategies for defensible annual sums of net ecosystem exchange, *Agric. For. Meteorol.*, *107*, 43–69.
Fan, X., B. Pedroli, G. Liu, Q. Liu, H. Liu, and L. Shu (2012), Soil salinity development in the Yellow River Delta in relation to groundwater dynamics, *Land Degrad. Dev.*, *23*, 175–189.
Foken, T., and B. Wichura (1996), Tools for quality assessment of surface based flux measurements, *Agric. For. Meteorol.*, *78*, 83–105.
Han, G., Q. Xing, Y. Luo, R. Rafique, J. Yu, and N. Mikle (2014a), Vegetation types alter soil respiration and its temperature sensitivity at the field scale in an estuary wetland, *PLoS One*, *9*(3), e91182.
Han, G., Q. Xing, J. Yu, Y. Luo, D. Li, L. Yang, G. Wang, P. Mao, B. Xie, and N. Mikle (2014b), Agricultural reclamation effects on ecosystem CO_2 exchange of a coastal wetland in the Yellow River Delta, *Agric. Ecosyst. Environ.*, *196*, 187–198.
Hao, Y. B., X. Y. Cui, Y. F. Wang, X. R. Mei, X. M. Kang, N. Wu, P. Luo, and D. Zhu (2011), Predominance of precipitation and temperature controls on ecosystem CO_2 exchange in Zoige alpine wetlands of southwest China, *Wetlands*, *31*, 413–422.
Hidding, B., J. M. Sarneel, and E. S. Bakker (2014), Flooding tolerance and horizontal expansion of wetland plants: Facilitation by floating mats?, *Aquat. Bot.*, *113*, 83–89.
Hirano, T., H. Segah, T. Harada, S. Limin, T. June, R. Hirata, and M. Osaki (2007), Carbon dioxide balance of a tropical peat swamp forest in Kalimantan, Indonesia, *Global Change Biol.*, *13*, 412–425.
Humphreys, E. R., P. M. Lafleur, L. B. Flanagan, N. Hedstrom, K. H. Syed, A. J. Glenn, and R. Granger (2006), Summer carbon dioxide and water vapor fluxes across a range of northern peatlands, *J. Geophys. Res.*, *111*, G04011, doi:10.1029/2005JG00011.
Jacobs, C. M. J., A. F. G. Jacobs, F. C. Bosveld, D. M. D. Hendriks, A. Hensen, P. Kroon, E. J. Moors, L. Nol, A. Schrier-Uijl, and E. M. Veenendaal (2007), Variability of annual CO_2 exchange from Dutch grasslands, *Biogeosciences*, *4*, 803–816.
Jimenez, K. L., G. Starr, C. L. Staudhammer, J. L. Schedlbauer, H. W. Loescher, S. L. Malone, and S. F. Oberbauer (2012), Carbon dioxide exchange rates from short- and long-hydroperiod Everglades freshwater marsh, *J. Geophys. Res.*, *117*, G04009, doi:10.1029/2012JG002117.
Kaimal, J. C., and J. J. Finnigan (1994), *Atmospheric Boundary Layer Flows: Their Structure and Measurement*, 289 pp., Oxford Univ. Press, Oxford, U. K.
Kang, X., Y. Wang, H. Chen, J. Tian, X. Cui, Y. Rui, L. Zhong, P. Kardol, Y. Hao, and X. Xiao (2014), Modeling carbon fluxes using multi-temporal MODIS imagery and CO_2 eddy flux tower data in Zoige alpine wetland, south-west China, *Wetlands*, *34*, 603–618.
Kathilankal, J. C., T. J. Mozdzer, J. D. Fuentes, P. D'Odorico, K. J. McGlathery, and J. C. Zieman (2008), Tidal influences on carbon assimilation by a salt marsh, *Environ. Res. Lett.*, *3*, 044010.
Kayranli, B., M. Scholz, A. Mustafa, and A. Hedmark (2010), Carbon storage and fluxes within freshwater wetlands: A critical review, *Wetlands*, *30*, 111–124.
Knox, S. H., C. Sturtevant, J. H. Matthes, L. Koteen, J. Verfaillie, and D. Baldocchi (2015), Agricultural peatland restoration: Effects of land-use change on greenhouse gas (CO_2 and CH_4) fluxes in the Sacramento-San Joaquin Delta, *Global Change Biol.*, *21*, 750–765.
Kosugi, Y., S. Takanashi, S. Ohkubo, N. Matsuo, M. Tani, T. Mitani, D. Tsutsumi, and A. R. Nik (2008), CO_2 exchange of a tropical rainforest at Pasoh in Peninsular Malaysia, *Agric. For. Meteorol.*, *148*, 439–452.
Kundzewicz, Z. W., et al. (2014), Flood risk and climate change: Global and regional perspectives, *Hydrol. Sci. J.*, *59*, 1–28.
Lafleur, P. M., N. T. Roulet, J. L. Bubier, S. Frolking, and T. R. Moore (2003), Interannual variability in the peatland-atmosphere carbon dioxide exchange at an ombrotrophic bog, *Global Biogeochem. Cycles*, *17*(2), 1036, doi:10.1029/2002GB001983.
Law, B. E., P. E. Thornton, J. Irvine, P. M. Anthoni, and S. Van Tuyl (2001), Carbon storage and fluxes in ponderosa pine forests at different developmental stages, *Global Change Biol.*, *7*, 755–777.
Lei, H. M., and D. W. Yang (2010), Seasonal and interannual variations in carbon dioxide exchange over a cropland in the North China Plain, *Global Change Biol.*, *16*, 2944–2957.
Li, S., G. Wang, W. Deng, Y. Hu, and W. Hu (2009), Influence of hydrology process on wetland landscape pattern: A case study in the Yellow River Delta, *Ecol. Eng.*, *35*, 1719–1726.
Lloyd, J., and J. A. Taylor (1994), On the temperature dependence of soil respiration, *Funct. Ecol.*, *8*, 315–323.
Lund, M., et al. (2010), Variability in exchange of CO_2 across 12 northern peatland and tundra sites, *Global Change Biol.*, *16*, 2436–2448.
McNicol, G., and W. L. Silver (2014), Separate effects of flooding and anaerobiosis on soil greenhouse gas emissions and redox sensitive biogeochemistry, *J. Geophys. Res. Biogeosci.*, *119*, 557–566, doi:10.1002/2013JG002433.
Merbold, L., et al. (2009), Precipitation as driver of carbon fluxes in 11 African ecosystems, *Biogeosciences*, *6*, 1027–1041.
Millennium Ecosystem Assessment (2005), *Ecosystems and Human Well-Being: Wetlands and Water Synthesis*, World Resour. Inst., Washington, D. C.
Mitsch, W. J., and J. G. Gosselink (2007), *Wetlands*, 4th ed., John Wiley, New York.
Mitsch, W. J., A. M. Nahlik, B. Bernal, L. Zhang, C. J. Anderson, S. E. Jörgensen, U. Mander, and H. Brix (2013), Wetlands, carbon, and climate change, *Landscape Ecol.*, *28*, 583–597.
Moffett, K. B., A. Wolf, J. A. Berry, and S. M. Gorelick (2010), Salt marsh–atmosphere exchange of energy, water vapor, and carbon dioxide: Effects of tidal flooding and biophysical controls, *Water Resour. Res.*, *46*, W10525, doi:10.1029/2009WR009041.
Paul, S., K. Jusel, and C. Alewell (2006), Reduction processes in forest wetlands: Tracking down heterogeneity of source/link functions with a combination of methods, *Soil Biol. Biochem.*, *38*, 1028–1039.
Pelletier, L., M. Garneau, and T. R. Moore (2011), Variation in CO_2 exchange over three summers at microform scale in a boreal bog, Eastmain region, Québec, Canada, *J. Geophys. Res.*, *116*, G03019, doi:10.1029/2011JG001657.
Polley, H. W., A. B. Frank, J. Sanabria, and R. L. Phillips (2008), Interannual variability in carbon dioxide fluxes and flux-climate relationships on grazed and ungrazed northern mixed-grass prairie, *Global Change Biol.*, *14*, 1620–1632.
Riutta, T., J. Laine, and E. S. Tuittila (2007), Sensitivity of CO_2 exchange of fen ecosystem components to water level variation, *Ecosystems*, *10*, 718–733.
Rocha, A. V., and M. L. Goulden (2008), Large interannual CO_2 and energy exchange variability in a freshwater marsh under consistent environmental conditions, *J. Geophys. Res.*, *113*, G04019, doi:10.1029/2008JG000712.
Sagerfors, J., A. Lindroth, A. Grelle, L. Klemedtsson, P. Weslien, and M. Nilsson (2008), Annual CO_2 exchange between a nutrient-poor, minerotrophic, boreal mire and the atmosphere, *J. Geophys. Res.*, *113*, G01001, doi:10.1029/2006JG000306.
Sairam, R. K., D. Kumutha, K. Ezhilmathi, P. S. Deshmukh, and G. C. Srivastava (2008), Physiology and biochemistry of waterlogging tolerance in plants, *Biol. Plant.*, *52*(3), 401–412.
Schedlbauer, J. L., S. F. Oberbauer, G. Starr, and K. L. Jimenez (2010), Seasonal differences in the CO_2 exchange of a short-hydroperiod Florida Everglades marsh, *Agric. For. Meteorol.*, *150*, 994–1006.
Sulman, B. N., A. R. Desai, N. Z. Saliendra, P. M. Lafleur, L. B. Flanagan, O. Sonnentag, D. S. Mackay, A. G. Barr, and G. van der Kamp (2010), CO_2 fluxes at northern fens and bogs have opposite responses to inter-annual fluctuations in water table, *Geophys. Res. Lett.*, *37*, L19702, doi:10.1029/2010GL044018.

Syed, K. H., L. B. Flanagan, P. J. Carlson, A. J. Glenn, and K. E. van Gaalen (2006), Environmental control of net ecosystem CO_2 exchange in a treed, moderately rich fen in northern Alberta, *Agric. For. Meteorol.*, *140*, 97–114.

Teklemariam, T. A., P. M. Lafleur, T. R. Moore, N. T. Roulet, and E. R. Humphreys (2010), The direct and indirect effects of inter-annual meteorological variability on ecosystem carbon dioxide exchange at a temperate ombrotrophic bog, *Agric. For. Meteorol.*, *150*, 1402–1411.

Tong, C., C. Wang, J. F. Huang, W. Q. Wang, Y. E, J. Liao, and C. Yao (2014), Ecosystem respiration does not differ before and after tidal inundation in Brackish Marshes of the Min River Estuary, southeast China, *Wetlands*, *34*, 225–233.

Urbanski, S., C. Barford, S. Wofsy, C. Kucharik, E. Pyle, J. Budney, K. McKain, D. Fitzjarrald, M. Czikowsky, and J. W. Munger (2007), Factors controlling CO_2 exchange on timescales from hourly to decadal at Harvard Forest, *J. Geophys. Res.*, *112*, G02020, doi:10.1029/2006JG000293.

Vogel, S. (1994), *Life in Moving Fluids: The Physical Biology of Flow*, Princeton Univ. Press, Princeton, N. J.

Webb, E. K., G. I. Pearman, and R. Leuning (1980), Correction of flux measurements for density effects due to heat and water vapor transport, *Q. J. R. Meteorol. Soc.*, *106*, 85–100.

Xie, X., M. Q. Zhang, B. Zhao, and H. Q. Guo (2014), Dependence of coastal wetland ecosystem respiration on temperature and tides: A temporal perspective, *Biogeosciences*, *11*, 539–545.

Yan, Y. E., H. Q. Guo, Y. Gao, B. Zhao, J. Q. Chen, B. Li, and J. K. Chen (2010), Variations of net ecosystem CO_2 exchange in a tidal inundated wetland: Coupling MODIS and tower-based fluxes, *J. Geophys. Res.*, *115*, D15102, doi:10.1029/2009JD012838.

Yang, M., S. Liu, Z. Yang, T. Sun, S. D. DeGloria, and K. Holt (2009), Effect on soil properties of conversion of Yellow River Delta ecosystems, *Wetlands*, *29*, 1014–1022.

Yao, R. J., and J. S. Yang (2010), Quantitative evaluation of soil salinity and its spatial distribution using electromagnetic induction method, *Agric. Water Manage.*, *97*, 1961–1970.

Yurova, A., A. Wolf, J. Sagerfors, and M. Nilsson (2007), Variations in net ecosystem exchange of carbon dioxide in a boreal mire: Modeling mechanisms linked to water table position, *J. Geophys. Res.*, *112*, G02025, doi:10.1029/2006JG000342.

Zhang, T. T., S. L. Zeng, Y. Gao, Z. T. Ouyang, B. Li, C. M. Fang, and B. Zhao (2011), Assessing impact of land uses on land salinization in the Yellow River Delta, China using an integrated and spatial statistical model, *Land Use Policy*, *28*, 857–866.

Zhou, L., G. Zhou, and Q. Jia (2009), Annual cycle of CO_2 exchange over a reed (*Phragmites australis*) wetland in northeast China, *Aquat. Bot.*, *91*, 91–98.